

Halogen partitioning and structural incorporation in K- and Na-jarosite: Experimental insights under Mars-relevant conditions

Rui CHANG¹, Yu-Yan Sara ZHAO (✉)^{2,3}

¹ Key Laboratory of Planetary Science and Frontier Technology, Institute of Geology and Geophysics, Chinese Academy of Sciences, Beijing 100029, China

² Research Center for Planetary Science, College of Earth and Planetary Sciences, Chengdu University of Technology, Chengdu 610059, China

³ CAS Center for Excellence in Comparative Planetology, Hefei 230026, China

© The Author(s) 2025. Published by Higher Education Press. This is an open access article under the CC BY license (<http://creativecommons.org/licenses/by/4.0>)

Abstract Jarosite is an important Martian sulfate mineral with the potential to record the physicochemical conditions and fluid evolution of aqueous environments on Mars. Previous studies suggest that jarosite can incorporate trace halogens such as bromide (Br^-), offering insights into paleo-fluid composition and halogen cycling on early Mars. However, the mechanisms governing halogen incorporation remain poorly constrained. In this study, we systematically examined K- and Na-jarosite synthesized from Br^-/Cl^- -bearing solutions prepared via two distinct pathways: Fe^{2+} oxidation at 25 °C and Fe^{3+} hydrolysis at 140 °C. Building on previous studies of low-temperature K-jarosite, we broadened the dataset to include both K- and Na-jarosite synthesized via Fe^{2+} oxidation and Fe^{3+} hydrolysis, and performed integrated chemical, crystallographic, and spectroscopic analyses to assess halogen uptake and substitution mechanisms. Our results show that Br^- is preferentially incorporated into K-jarosite, particularly under low-temperature conditions, with solid-liquid partition ratios ($C_{\text{s-Br}}/C_{\text{aq-Br}}$) exceeding 18. In contrast, Na-jarosite remains halogen-poor and exhibits structurally Fe deficiency across all tested conditions. Collectively, Raman spectroscopy, XRD lattice contraction, and stoichiometric data indicate that Br^- and Cl^- primarily substitute for structural OH^- groups, with maximal substitution in low-temperature K-jarosite. Halogen incorporation is strongly controlled by the A-site cation and synthesis pathways, with K-jarosite accommodating far more halogen than Na-jarosite. Low-temperature conditions may promote Br^- uptake via defect trapping and slower crystallization kinetics, whereas

hydrothermal synthesis enhances crystallinity but reduces halogen incorporation. The Br^- enrichment in jarosite parallels that observed in kainite-type double salts, suggesting that jarosite can act as a selective Br^- sink in oxidizing acidic systems. On Mars, Br-bearing jarosite may reflect formation in low-temperature, chemically evolved brines. These findings underscore the dual role of jarosite as both paleoenvironmental proxy and an active participant in halogen cycling. Variations in halogen content, crystallinity, and lattice parameters may provide valuable constraints for reconstructing aqueous histories in future returned Martian samples.

Keywords jarosite, natrojarosite, Br/Cl ratio, sulfate, double salt.

1 Introduction

Jarosite is an important component of the Burns Formation outcrop at Meridiani Planum, Mars (Klingelhöfer et al., 2004; Morris et al., 2006), and has been detected both in situ and from orbit at other locations across the Martian surface, including Gale Crater, the Valles Marineris canyon system, and Mawrth Vallis (Farrand et al., 2009; Liu et al., 2018; Milliken et al., 2008; Rampe et al., 2020; Rampe et al., 2017). Due to its strong indication of oxidizing aqueous condition and inherent instability in fluid environments, the presence of jarosite in Martian sedimentary rocks is widely regarded as a key indicator of the aqueous geochemistry and hydrological history of early Mars (e.g., Madden et al., 2004). In recent years, studies have progressed beyond detection efforts, shifting focus toward understanding the formation mechanisms,

transformation pathways, and paleoenvironmental significance of jarosite under simulated Martian conditions, often in conjunction with terrestrial analog site investigations (Belleau-Magnat et al., 2025; Carson et al., 2023; Hong et al., 2024; Grasby et al., 2022; Knight et al., 2024). Furthermore, jarosite is a promising geochronometer for future returned Martian samples, as its structural K^+ incorporation enables K-Ar dating to constrain the timing of past aqueous alteration events on Mars (Martin et al., 2017; Papike et al., 2006; Ren and Vasconcelos, 2020).

Natural jarosite-group minerals have a general formula $AFe_3(SO_4)_2(OH)_6$, where the A-site is a 12-fold coordinated position occupied by monovalent or divalent cations (commonly K^+ , Na^+ and H_3O^+). This site defines three primary endmembers: K-jarosite ($KFe_3(SO_4)_2(OH)_6$), natrojarosite ($NaFe_3(SO_4)_2(OH)_6$), and hydronium jarosite ($(H_3O)Fe_3(SO_4)_2(OH)_6$). The jarosite mineral group is known for its structural flexibility, accommodating a wide range of elements across the periodic table (Papike et al., 2006). Our group has conducted a series of experimental studies examining the incorporation behavior of halide anions, particularly bromide (Br^-) and chloride (Cl^-), during jarosite formation under low-temperature, Mars-relevant aqueous conditions (Chang and Zhao, 2018; Zhao et al., 2014). Previous results demonstrate that jarosite exhibits strong preferential uptake of Br^- over Cl^- during Fe^{2+} oxidation and precipitation at ambient temperature. When initial solution concentrations are equal, Br^- incorporation efficiency exceeds that of Cl^- by up to two orders of magnitude. This selective partitioning results in Br-enriched jarosite, offering a potentially explanation for the elevated Br/Cl ratios detected in Martian sediments and supporting the hypothesis that jarosite may act as a significant Br reservoir on the Martian surface (Chang and Zhao, 2018). Moreover, halogen incorporation appears to influence the aqueous stability of jarosite, with Br- and Cl^- -bearing phases showing distinct dissolution behaviors under various geochemical conditions (Zhao et al., 2014; Zhou et al., 2022). These findings underscore the dual role of halogens in modulating both the compositional and diagenetic signatures of jarosite, thereby refining our understanding of water-rock interactions and the persistence of aqueous environments on Mars.

However, several key questions remain unresolved regarding halogen behavior during jarosite formation. First, it is unclear whether the Br^- preference observed in K-jarosite also applies to the Na-jarosite endmember. Second, the influence of temperature conditions on Br^- enrichment is poorly constrained, particularly whether low-temperature (e.g., 25 °C) and hydrothermal (e.g., 140 °C) conditions yield different halogen incorporation efficiencies. Finally, the structural consequences of halide substitution are not well understood, including the specific occupancy of Br^- and Cl^- within the jarosite

lattice (e.g., hydroxyl (OH^-) vs. interlayer sites), and the potential lattice parameter modifications at elevated halogen concentrations. Resolving these issues is essential for interpreting halogen-bearing jarosite detected on Mars and assessing its utility as a geochemical proxy for past aqueous processes.

Building on our demonstration of appreciable Br^- incorporation in K-jarosite precipitated at ambient temperature (Chang and Zhao, 2018), this study systematically investigates the halide partitioning behavior and its structural consequences. We synthesized a suite of halogen-bearing K- and Na-jarosite samples across a range of initial Br^- and Cl^- concentrations under both room-temperature (25 °C) and hydrothermal (140 °C) conditions. Structural characterizations were performed to identify halide occupancy sites and assess their effects on crystallography. These results provide key constraints on Br^- enrichment mechanisms in Martian jarosite and advance the reconstruction of paleo-brine compositions from ancient halogen signatures.

2 Experimental Methods

2.1 Jarosite samples

2.1.1 Synthesis of K- and Na-jarosite at 25 °C

Jarosite samples were synthesized at room temperature (25 °C) following a modified low-temperature Fe(II) oxidation method same as that described in Chang and Zhao (2018). Endmembers of K-jarosite and Na-jarosite were both prepared to investigate halogen partitioning behavior under comparable aqueous conditions. For each endmember, four types of jarosite were synthesized, including halogen-free, Br-only, Cl-only, and Br, Cl^- -bearing.

In all experiments, Fe^{2+} was introduced as $FeSO_4 \cdot 7H_2O$ dissolved in 454 mL of 0.45 M $MgSO_4$ solution in a 1 L beaker. For K-jarosite synthesis, 100 g $FeSO_4 \cdot 7H_2O$ was used, whereas Na-jarosite synthesis required 258 g to suppress goethite formation and ensure natrojarosite purity, as established in preliminary trials. Halogen-bearing experiments included KCl or KBr (K-jarosite) and NaCl or NaBr (Na-jarosite), while halogen-free controls used 3.00 g K_2SO_4 or 2.43 g Na_2SO_4 as cation sources.

For Cl-only and Br-only jarosite syntheses, a range of initial halide concentrations was used to assess the effects of halogen content on jarosite formation. In the K-jarosite system, SO_4^{2-}/Cl^- molar ratios were set at 4, 3, 2, and 1, corresponding to initial Cl^- concentrations of 0.76 to 2.91 wt.%. For bromide, SO_4^{2-}/Br^- molar ratios were set at 8, 6, 4, and 2, yielding Br^- concentrations of 0.86 to 3.32 wt.%. Na-jarosite synthesis required more $FeSO_4 \cdot 7H_2O$

than K-jarosite to promote pure natrojarosite formation and suppress goethite precipitation, resulting in a higher initial sulfate concentration. Halide concentrations were kept the same as in the K-jarosite experiments (0.62 of Cl^- ; 0.60 to 2.34 wt.% of Br^-). Therefore, the elevated sulfate led to higher initial molar ratios of $\text{SO}_4^{2-}/\text{Cl}^-$ (i.e., 8) and $\text{SO}_4^{2-}/\text{Br}^-$ (i.e., 16, 12, 8, and 4).

For Br, Cl^- -bearing runs, initial $\text{SO}_4^{2-}/\text{Cl}^-$ molar ratios were fixed at 2 for K-jarosite and 4 for Na-jarosite, while Br^- concentrations were adjusted to yield Cl^-/Br^- molar ratios of 2, 4, 10, 25, and 50. This corresponded to initial Br^- concentrations of 0.07 to 1.65 wt.% (K-jarosite) and 0.06 to 1.38 wt.% (Na-jarosite).

All syntheses were conducted in 1 L beakers covered with parafilm perforated by a 2 cm hole to allow atmospheric oxidation of Fe^{2+} . Suspensions were stirred continuously for 15 days. At the end of each run, solids were collected by centrifugation, washed three times with 18.2 M Ω ultrapure water (Milli-Q), and air-dried in a fume hood. Solution pH was measured at the beginning and end of the experiments. All reagents were ACS grade.

2.1.2 Synthesis of K- and Na-jarosite at 140 °C

Halogen-free K- and Na-jarosite endmembers were synthesized at 140 °C using the hydrothermal forced hydrolysis method of [Basciano and Peterson \(2008\)](#) and [Ling et al. \(2016\)](#).

For K-jarosite synthesis, 5 mL of 1.23 M FeCl_3 , 0.5 g KCl, and the designated amount of KBr (per Cl^-/Br^- ratios) were dissolved in 12 mL of saturated LiCl solution. Separately, 6.00 g $\text{Fe}_2(\text{SO}_4)_3 \cdot 5\text{H}_2\text{O}$ was dissolved in 25 mL ultrapure water and slowly added to the chloride solution under continuous stirring. For Na-jarosite, 5 mL of 1.23 M FeCl_3 , 0.5 g NaCl, and the corresponding amount of NaBr were dissolved in 12 mL saturated LiCl, while 6.00 g $\text{Fe}_2(\text{SO}_4)_3 \cdot 5\text{H}_2\text{O}$ and 0.85 g Na_2SO_4 were dissolved in 25 mL ultrapure water and added in the same manner. The mixtures were sealed in Teflon-lined autoclaves, heated at 140 °C for 48 h, cooled to room temperature, centrifuged, washed three times with ultrapure water, and dried at 75 °C. Initial Cl^-/Br^- molar ratios of 100, 50, 25, 10, and 4 were prepared with Cl^- fixed at ~9.0 wt.% and Br^- varied from 0.19 to 4.53 wt.% for K-jarosite and 0.19 to 4.50 wt.% for Na-jarosite.

Because hydrothermal synthesis at 140 °C necessarily uses FeCl_3 , Cl^- cannot be completely excluded. To obtain halogen-free jarosite for comparison, additional K- and Na-jarosite were synthesized at 90 °C following [Driscoll and Leinz \(2005\)](#). In each case, 17.20 g $\text{Fe}_2(\text{SO}_4)_3 \cdot n\text{H}_2\text{O}$ was dissolved in 100 mL ultrapure water, followed by 5.60 g KOH (K-jarosite) or 4.00 g NaOH (Na-jarosite). Beakers were covered and heated at 90 °C with stirring for 4 h. The solids were recovered by filtration, rinsed three times with ultrapure water, and dried at 110 °C for 24 h.

2.2 Analytical methods

Synthesized jarosite samples were characterized using multiple techniques, including Powder X-ray diffraction (XRD), Raman spectroscopy, X-ray fluorescence (XRF), and scanning electron microscopy coupled with energy-dispersive X-ray spectroscopy (SEM-EDS), the sulfur-carbon analyzer, atomic absorption spectrophotometry (AAS), and ion chromatography (IC).

XRD data were first collected using a Panalytical Empyrean diffractometer (45 kV, 40 mA) with $\text{Cu-K}\alpha$ radiation ($\lambda = 1.5419 \text{ \AA}$), scanning from 10° to $60^\circ 2\theta$ with a step size of 0.0263° and a counting time of 36.465 s per step. High-resolution XRD Rietveld refinements were performed on selected samples to determine crystallographic parameters. The high-resolution XRD analyses were conducted at the Shanghai Institute of Ceramics, CAS, using a Bruker D8 Advance diffractometer with $\text{Cu-K}\alpha$ radiation, scanning 13° – $110^\circ 2\theta$ with a step size of 0.02° and a counting time of 0.8 s per step.

Raman spectra were acquired at the Institute of Geochemistry, Chinese Academy of Sciences, using a Renishaw InVia confocal micro-Raman spectrometer, with a $20\times$ objective lens and a 532 nm laser, over a spectral range of 100 to 4000 cm^{-1} .

Halogen contents were quantified by XRF (SHIMADZU XRF-1800X) at East China Normal University. Calibration standards were prepared to closely match the target halogen concentrations in the samples, following procedures described in [Zhao et al. \(2014\)](#). The standards consisted of crystal violet, Fe_2O_3 , KBr, and Na_2SO_4 mixtures. Detection limits were 0.35 wt.% for Br and 0.67 wt.% for Cl.

SEM-EDS observations were performed at the Institute of Geochemistry, Chinese Academy of Sciences, using a FEI Scios dual-beam SEM equipped with an ETD detector, operated at 20 kV and a working distance of 1.9–7.0 mm.

The sulfur content was analyzed at ALS Geochemistry (Guangzhou) using a LECO sulfur-carbon analyzer. Samples were combusted in an induction furnace at 1350 °C to convert sulfur SO_2 gas, which was quantified by an infrared detection system. Analytical precision was better than $\pm 2.5\%$ (relative) and accuracy better than $\pm 1.77\%$ (relative).

Major cations (Na, K, Fe, Mg, Li) of the synthetic jarosite samples were determined by AAS following complete sample digestion. For aqueous solutions, anions (Cl^- , Br^- , and SO_4^{2-}) were quantified by IC and cations by AAS, with all measurements performed in triplicate. Standard errors for IC measurements were 1.19% (Br^-), 2.46% (Cl^-), and 2.04% (SO_4^{2-}). For cations, standard errors ranged from $\pm 1.14\%$ to $\pm 1.61\%$ (average $\pm 1.32\%$). Unless otherwise specified, all analysis were performed at the Institute of Geochemistry, Chinese Academy of Sciences.

3 Results

3.1 Compositional characteristics of synthetic halogen-bearing jarosite

All synthetic samples were confirmed as pure jarosite by

powder XRD and Raman spectroscopy, with no secondary phases detected by SEM-EDS (see Section 3.3). The chemical compositions and calculated formulas of K- and Na-jarosite are listed in Tables 1 and 2, respectively. Halogen-free K- and Na-jarosite samples synthesized at 90 °C contained no Cl⁻ contamination were also shown in Table 2, and serve as reference

Table 1 Chemical compositions of K- and Na-jarosite produced by Fe²⁺ oxidation at 25 °C

K-jarosite ^a	Target settings (molar ratios)	Initial solutions		Final solutions		Jarosite solids					Partitioning		Formula	
		Br wt.%	Cl wt.%	Br wt.%	Cl wt.%	Br wt.%	Cl wt.%	S wt.%	K wt.%	Fe wt.%	Mg mg/kg	C _{s-Br} /C _{aq-Br}		C _{s-Cl} /C _{aq-Cl}
K-blank-25C	blank	–	–	–	–	–	–	13.3	6.8	27.5	54.4	–	–	(K _{0.84} H ₃ O _{0.16})Fe _{2.38} (SO ₄) ₂ (OH) ₆
K-Br-01	SO ₄ /Br = 8	0.86	–	0.90	–	5.34	–	13.4	7.2	27.4	21.6	5.9	–	(K _{0.88} H ₃ O _{0.12})Fe _{2.35} (SO ₄) ₂ (OH) _{5.68} Br _{0.32}
K-Br-02	SO ₄ /Br = 6	1.15	–	1.16	–	6.34	–	13.6	7.3	27.3	22.0	5.5	–	(K _{0.87} H ₃ O _{0.13})Fe _{2.30} (SO ₄) ₂ (OH) _{5.63} Br _{0.37}
K-Br-03	SO ₄ /Br = 4	1.70	–	1.69	–	8.04	–	13.2	7.3	26.7	23.1	4.7	–	(K _{0.90} H ₃ O _{0.10})Fe _{2.32} (SO ₄) ₂ (OH) _{5.51} Br _{0.49}
K-Br-04	SO ₄ /Br = 2	3.32	–	2.90	–	11.24	–	13.4	7.5	26.8	25.5	3.9	–	(K _{0.92} H ₃ O _{0.08})Fe _{2.29} (SO ₄) ₂ (OH) _{5.33} Br _{0.67}
K-Br,Cl-01	S/Cl = 8/4; Cl/Br = 50	0.07	1.46	0.05	1.34	1.06	0.26*	13.2	7.5	26.7	27.6	20.1	0.2	(K _{0.94} H ₃ O _{0.06})Fe _{2.33} (SO ₄) ₂ (OH) _{5.94} Br _{0.06} Cl _{0.04}
K-Br,Cl-02	S/Cl = 8/4; Cl/Br = 25	0.14	1.48	0.10	1.45	1.80	0.25*	13.0	7.6	26.7	26.9	18.3	0.2	(K _{0.95} H ₃ O _{0.05})Fe _{2.36} (SO ₄) ₂ (OH) _{5.85} Br _{0.11} Cl _{0.03}
K-Br,Cl-03	S/Cl = 8/4; Cl/Br = 10	0.34	1.49	0.29	1.51	3.27	0.21*	13.3	7.4	27.2	89.0	11.3	0.1	(K _{0.92} H ₃ O _{0.08})Fe _{2.36} (SO ₄) ₂ (OH) _{5.77} Br _{0.20} Cl _{0.03}
K-Br,Cl-04	S/Cl = 8/4; Cl/Br = 4	0.84	1.50	0.80	1.59	5.68	0.19*	13.5	7.5	26.6	28.8	7.1	0.1	(K _{0.92} H ₃ O _{0.08})Fe _{2.27} (SO ₄) ₂ (OH) _{5.64} Br _{0.34} Cl _{0.03}
K-Br,Cl-05	S/Cl = 8/4; Cl/Br = 2	1.65	1.50	1.70	1.52	7.66	0.15*	13.1	7.5	26.5	27.3	4.5	0.1	(K _{0.94} H ₃ O _{0.06})Fe _{2.33} (SO ₄) ₂ (OH) _{5.51} Br _{0.47} Cl _{0.02}
K-Cl-01	SO ₄ /Cl = 4	–	0.76	–	0.79	–	0.17*	13.2	7.4	27.3	21.9	–	0.2	(K _{0.92} H ₃ O _{0.08})Fe _{2.38} (SO ₄) ₂ (OH) _{5.98} Cl _{0.02}
K-Cl-02	SO ₄ /Cl = 3	–	1.01	–	1.05	–	0.22*	13.0	7.4	26.9	24.5	–	0.2	(K _{0.93} H ₃ O _{0.07})Fe _{2.37} (SO ₄) ₂ (OH) _{5.97} Cl _{0.03}
K-Cl-03	SO ₄ /Cl = 2	–	1.50	–	1.57	–	0.29*	13.2	7.6	26.5	26.0	–	0.2	(K _{0.95} H ₃ O _{0.05})Fe _{2.31} (SO ₄) ₂ (OH) _{5.96} Cl _{0.04}
K-Cl-04	SO ₄ /Cl = 1	–	2.91	–	3.04	–	0.42*	13.0	7.6	26.1	30.2	–	0.1	(K _{0.96} H ₃ O _{0.04})Fe _{2.30} (SO ₄) ₂ (OH) _{5.94} Cl _{0.06}
Na-jarosite	Target settings (molar ratio)	Initial solutions		Final solutions		Jarosite solids					Partitioning		Formula	
		Br wt.%	Cl wt.%	Br wt.%	Cl wt.%	Br wt.%	Cl wt.%	S wt.%	Na wt.%	Fe wt.%	Mg mg/kg	C _{s-Br} /C _{aq-Br}		C _{s-Cl} /C _{aq-Cl}
Na-blank-25C	blank	–	–	–	–	–	–	13.5	3.4	13.1	302.0	–	–	(Na _{0.70} H ₃ O _{0.30})Fe _{1.11} (SO ₄) ₂ (OH) ₆
Na-Br-01	SO ₄ /Br = 16	0.60	–	0.62	–	0.14*	–	13.5	4.1	12.8	240.1	0.2	–	(Na _{0.84} H ₃ O _{0.16})Fe _{1.09} (SO ₄) ₂ (OH) _{5.99} Br _{0.01}
Na-Br-02	SO ₄ /Br = 12	0.80	–	0.83	–	0.22*	–	13.4	4.0	13.3	403.2	0.3	–	(Na _{0.83} H ₃ O _{0.17})Fe _{1.15} (SO ₄) ₂ (OH) _{5.99} Br _{0.01}
Na-Br-03	SO ₄ /Br = 8	1.19	–	1.44	–	0.53	–	13.4	3.9	13.7	376.3	0.4	–	(Na _{0.81} H ₃ O _{0.19})Fe _{1.18} (SO ₄) ₂ (OH) _{5.97} Br _{0.03}
Na-Br-04	SO ₄ /Br = 4	2.34	–	2.83	–	0.79	–	13.4	3.9	14.9	324.0	0.3	–	(Na _{0.81} H ₃ O _{0.19})Fe _{1.28} (SO ₄) ₂ (OH) _{5.95} Br _{0.05}
Na-Br,Cl-01	S/Cl = 8/4; Cl/Br = 50	0.06	1.22	0.11	1.22	0.02*	0.02*	14.0	3.9	11.9	374.1	0.2	0	(Na _{0.77} H ₃ O _{0.23})Fe _{0.98} (SO ₄) ₂ (OH) ₆
Na-Br,Cl-02	S/Cl = 8/4; Cl/Br = 25	0.11	1.23	0.06	1.27	0.03*	0.01*	13.7	3.9	14.9	227.2	0.5	0	(Na _{0.79} H ₃ O _{0.21})Fe _{1.25} (SO ₄) ₂ (OH) ₆
Na-Br,Cl-03	S/Cl = 8/4; Cl/Br = 10	0.28	1.24	0.27	1.29	0.07*	0.01*	14.0	3.9	13.6	304.3	0.3	0	(Na _{0.78} H ₃ O _{0.22})Fe _{1.12} (SO ₄) ₂ (OH) ₆
Na-Br,Cl-04	S/Cl = 8/4; Cl/Br = 4	0.70	1.24	0.71	1.33	0.21*	0.03*	13.5	3.9	14.2	231.0	0.3	0	(Na _{0.80} H ₃ O _{0.20})Fe _{1.22} (SO ₄) ₂ (OH) _{5.98} Br _{0.02}
Na-Br,Cl-05	S/Cl = 8/4; Cl/Br = 2	1.38	1.24	1.46	1.30	0.43	0.08*	12.9	3.4	14.8	525.7	0.3	0.1	(Na _{0.73} H ₃ O _{0.27})Fe _{1.32} (SO ₄) ₂ (OH) _{5.96} Br _{0.03} Cl _{0.01}
Na-Cl-01	SO ₄ /Cl = 8	–	0.62	–	0.58	–	0.00*	13.8	3.9	17.1	377.6	–	0	(Na _{0.79} H ₃ O _{0.21})Fe _{1.43} (SO ₄) ₂ (OH) ₆

Notes: Br and Cl concentrations in the initial solutions increase with sample number. All reported values are based on measurements: halogens in solutions by ion chromatography (IC); Br and Cl in solids by XRF; Fe, K, Na, Mg by AAS after acid digestion; and total S by infrared C-S analysis. Analytical variations may cause minor uncertainties in stoichiometric calculations. Mg²⁺ incorporation was negligible (mg/kg level) and excluded from formula derivation. a. Compositional data for K-jarosite (25 °C) are from Chang and Zhao (2018), with formulas recalculated in this study considering H₃O⁺ as a possible A-site occupant. All formulas were normalized to two SO₄²⁻ per unit for consistency. *Asterisked values are below detection limits (0.35 wt.% Br; 0.67 wt.% Cl by XRF) but included due to their linear correlation with initial solution concentrations.

Table 2 Chemical compositions of K- and Na-jarosite synthesized via Fe³⁺ hydrolysis at 140 °C

K-jarosite	Target settings	Initial solutions		Final solutions		Jarosite solids					Partitioning		Formula	
		Br	Cl	Br	Cl	Br	Cl	S	K	Fe	Li	C _{s-Br} /C _{aq-Br}		C _{s-Cl} /C _{aq-Cl}
		wt.%	wt.%	wt.%	wt.%	wt.%	wt.%	wt.%	wt.%	wt.%	wt.%	mg/kg		
K-blank-90C	blank	–	–	–	–	–	–	13.1	7.1	26.6	–	–	–	(K _{0.89} H ₃ O _{0.11})Fe _{2.34} (SO ₄) ₂ (OH) ₆
K-01-140C	Cl/Br = 100	0.19	9.07	0.11	9.52	0.08*	0.19*	13.1	7.0	21.7	661.2	0.8	0	(K _{0.88} H ₃ O _{0.08} Li _{0.05})Fe _{1.90} (SO ₄) ₂ (OH) _{5.97} Cl _{0.03}
K-02-140C	Cl/Br = 50	0.38	9.00	0.42	9.52	0.19*	0.22*	13.0	7.1	24.4	685.8	0.4	0	(K _{0.90} H ₃ O _{0.05} Li _{0.05})Fe _{2.16} (SO ₄) ₂ (OH) _{5.96} Br _{0.01} Cl _{0.03}
K-03-140C	Cl/Br = 25	0.77	9.05	0.79	9.28	0.41	0.27*	13.1	7.1	24.1	734.7	0.5	0	(K _{0.89} H ₃ O _{0.06} Li _{0.05})Fe _{2.11} (SO ₄) ₂ (OH) _{5.94} Br _{0.03} Cl _{0.04}
K-04-140C	Cl/Br = 10	1.88	8.84	1.81	9.26	1.09	0.33*	13.1	7.2	21.9	749.9	0.6	0	(K _{0.91} H ₃ O _{0.09} Li _{0.05})Fe _{1.93} (SO ₄) ₂ (OH) _{5.89} Br _{0.07} Cl _{0.05}
K-05-140C	Cl/Br = 4	4.53	8.49	4.66	8.61	2.94	0.48*	13.0	7.3	21.3	735.6	0.6	0.1	(K _{0.93} H ₃ O _{0.07} Li _{0.05})Fe _{1.88} (SO ₄) ₂ (OH) _{5.75} Br _{0.18} Cl _{0.07}
Na-jarosite	Target settings	Initial solutions		Final solutions		Jarosite solids					Partitioning		Formula	
		Br	Cl	Br	Cl	Br	Cl	S	Na	Fe	Li	C _{s-Br} /C _{aq-Br}		C _{s-Cl} /C _{aq-Cl}
		wt.%	wt.%	wt.%	wt.%	wt.%	wt.%	wt.%	wt.%	wt.%	wt.%	mg/kg		
Na-blank-90C	blank	–	–	–	–	–	–	12.2	3.3	16.2	–	–	–	(Na _{0.75} H ₃ O _{0.25})Fe _{1.53} (SO ₄) ₂ (OH) ₆
Na-01-140C	Cl/Br = 100	0.19	9.09	0.07	9.38	0.01*	0.00*	13.6	4.1	14.2	162.9	0.2	0	(Na _{0.83} H ₃ O _{0.15} Li _{0.01})Fe _{1.20} (SO ₄) ₂ (OH) ₆
Na-02-140C	Cl/Br = 50	0.38	9.06	0.41	9.45	0.01*	0.00*	13.7	4.1	12.0	281.6	0	0	(Na _{0.84} H ₃ O _{0.14} Li _{0.01})Fe _{1.01} (SO ₄) ₂ (OH) ₆
Na-03-140C	Cl/Br = 25	0.76	9.02	0.81	9.26	0.02*	0.00*	13.3	4.1	13.3	268.4	0	0	(Na _{0.86} H ₃ O _{0.12} Li _{0.01})Fe _{1.15} (SO ₄) ₂ (OH) ₆
Na-04-140C	Cl/Br = 10	1.87	8.89	2.00	9.16	0.03*	0.00*	13.8	4.0	12.1	296.3	0	0	(Na _{0.81} H ₃ O _{0.17} Li _{0.01})Fe _{1.01} (SO ₄) ₂ (OH) ₆
Na-05-140C	Cl/Br = 4	4.50	8.58	4.63	8.73	0.08*	0.00*	13.9	3.9	13.9	388.0	0	0	(Na _{0.79} H ₃ O _{0.19} Li _{0.01})Fe _{1.15} (SO ₄) ₂ (OH) ₆

Notes: Br and Cl concentrations in the initial solutions increase with sample number. All values are based on direct measurements: halogens in solutions by ion chromatography (IC); Br and Cl in solids by XRF; Fe, K, Na, and Li by AAS after acid digestion; and total S by infrared C-S analysis. Minor analytical uncertainties may affect stoichiometric calculations. Chemical formulas were normalized to two SO₄²⁻ per formula unit for consistent comparison. *Values marked with an asterisk are below detection limits (0.35 wt.% Br, 0.67 wt.% Cl by XRF) but are included due to their linear correlation with initial solution concentrations and use in formula calculations.

endmembers for evaluating halogen substitution effects.

3.1.1 Jarosite precipitated via Fe²⁺ oxidation at 25 °C

K-jarosite synthesized at 25 °C incorporated substantial Br⁻ under oxidative conditions. Initial Br⁻ concentrations ranged from 0.86 to 3.32 wt.% in Br-only and 0.07 to 1.65 wt.% in Br-Cl solutions, yielding up to 11.24 wt.%

Br in the solids with a strong positive correlation to solution Br (Fig. 1(a)). In contrast, Cl⁻ incorporation was minimal (0.02–0.06 wt.%) even at 2.91 wt.% initial Cl⁻ (Fig. 1(b)). In mixed-halogen systems, Cl⁻ uptake declined systematically with increasing Br/Cl ratios, indicating competitive substitution between Br⁻ and Cl⁻, consistent with previous findings (Chang and Zhao, 2018).

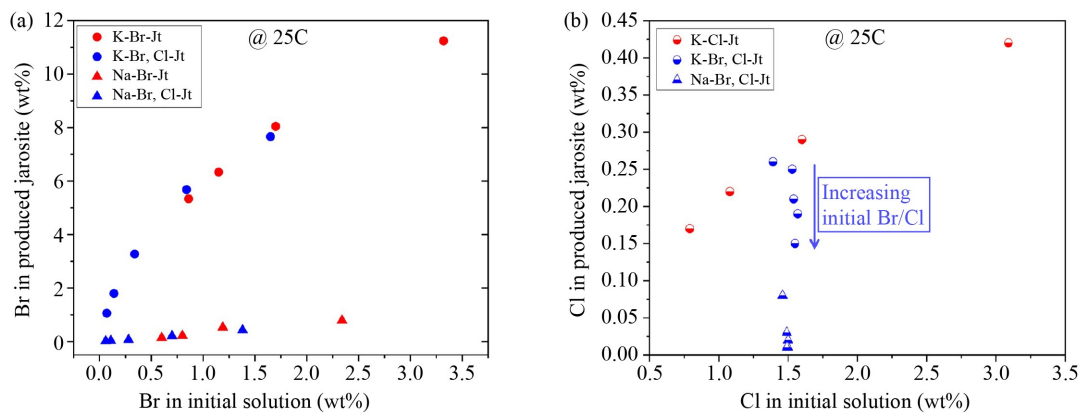


Fig. 1 Br and Cl incorporation into synthetic jarosite formed by Fe²⁺ oxidation at 25 °C as a function of initial solution concentrations. Br-only and Cl-only groups are in red; Br-Cl mixed groups in blue. (a) Br incorporation: K-jarosite (circles) shows strong positive correlation with initial Br, whereas Na-jarosite (triangles) remains < 1 wt.%. (b) Cl incorporation: K-jarosite reaches up to 0.42 wt.% in Cl-only systems but decreases in Br-Cl systems with higher Br/Cl ratios, indicating Br-Cl competition. Na-jarosite Cl contents are consistently below detection. Overall, jarosite preferentially incorporates Br⁻ over Cl⁻, and K-jarosite accommodates more halogens than Na-jarosite. Error bars are smaller than symbols.

For Na-jarosite, initial syntheses with 100 g $\text{FeSO}_4 \cdot 7\text{H}_2\text{O}$ produced goethite ($\alpha\text{-FeOOH}$) as a secondary phase. Increasing the $\text{FeSO}_4 \cdot 7\text{H}_2\text{O}$ to 280 g, while keeping other conditions constant, suppressed goethite formation and yielded pure Na-jarosite. Compared with K-jarosite, Na-jarosite incorporated much less halogen under similar conditions (Fig. 1), with Br contents ranging from below detection to a maximum of 0.79 wt.% despite solution Br concentrations up to 2.34 wt.% (Fig. 1(a)).

In Br-Cl experiments, Cl^- contents in Na-jarosite remained consistently low (≤ 0.08 wt.%; Fig. 1(b)). These results show that during low-temperature Fe^{2+} oxidation, both K- and Na-jarosite preferentially incorporate Br^- over Cl^- , with halogen uptake strongly controlled by the A-site cation, that K-jarosite accommodating far more halogen than Na-jarosite.

Note that the starting solutions contained 0.9 wt.% Mg^{2+} (K-jarosite) and 0.7 wt.% Mg^{2+} (Na-jarosite). At 25 °C, Mg contents in K-jarosite range from 21.6 to 89.0 mg/kg, with most values falling below 30 mg/kg, indicating only minor incorporation of Mg during low-temperature synthesis. In contrast, Na-jarosite samples display substantially higher Mg contents (227.2 to 525.7 mg/kg), consistently an order of magnitude greater than K-jarosite. This suggests either more effective incorporation of Mg^{2+} into Na-jarosite under the synthesis conditions or a higher affinity of the Na-jarosite structure for Mg impurities, despite Mg not being part of the ideal jarosite stoichiometry.

3.1.2 Jarosite synthesized by Fe^{3+} forced hydrolysis at 140 °C

Jarosite synthesized hydrothermally exhibited distinct halogen incorporation behavior. Because FeCl_3 was required as a starting material, initial Cl^- concentrations were consistently high (~8.49–9.09 wt.%). Br^- ranged from 0.19 to 4.53 wt.% (K-jarosite) and 0.19 to 4.50 wt.%

(Na-jarosite), defining different Cl/Br ratios. In K-jarosite solids, Br incorporation rose systematically with solution Br^- , reaching up to 2.94 wt.%, whereas Cl remained low (≤ 0.48 wt.%) despite elevated initial levels (Fig. 2(a)). This preferential Br^- uptake under hydrothermal conditions parallels room-temperature behavior, reflecting greater structural affinity of jarosite for Br^- .

In contrast, Na-jarosite at 140 °C incorporated only trace Br^- (≤ 0.08 wt.%) and virtually no Cl^- , despite high initial halogen levels (Fig. 2(b)). This confirms the limited capacity of Na-jarosite to host halogens, a trend consistent across both low- and high-temperature syntheses. This suppression is most evident for Cl^- , which was undetectable in all Na-jarosite samples. Such low Cl incorporation is consistent with previous reports showing jarosite synthesized from Cl-rich brines rarely exceeds 1 wt.% Cl (Basciano and Peterson, 2008; Driscoll and Leinz, 2005).

In addition, the hydrothermal solutions used for synthesizing halogen-bearing jarosite at 140 °C contained Li^+ at concentrations of approximately 2.6–2.9 wt.%. Although not a stoichiometric component of jarosite, a small but measurable amount of Li^+ was incorporated into both K- and Na-jarosite products. In K-jarosite, Li concentrations ranged from 661.2 to 749.9 mg/kg, whereas Na-jarosite contained 162.9 to 388.0 mg/kg. These results indicate limited but non-negligible Li substitution, possibly at the A-site.

Together, these observations demonstrate that even under hydrothermal conditions, Br^- is incorporated into jarosite more readily than Cl^- , and that the A-site cation (K^+ vs. Na^+) exerts a dominant control on halogen uptake efficiency.

3.2 Partitioning behavior of Br^- and Cl^- between solution and jarosite

The relative affinities of Br^- and Cl^- for incorporation

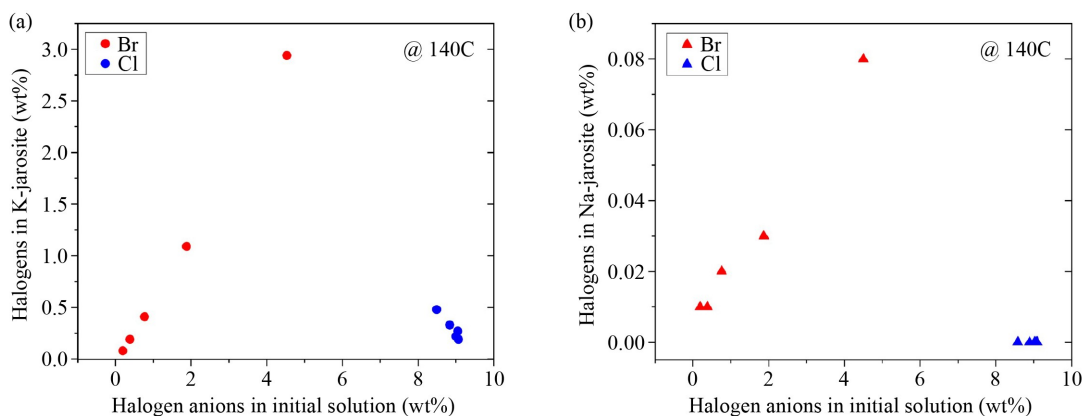


Fig. 2 Br and Cl incorporation into jarosite synthesized by Fe^{3+} hydrolysis at 140 °C as a function of initial Br-Cl solution composition. (a) K-jarosite shows increasing Br incorporation (up to 2.94 wt.%) with initial Br^- concentration, while Cl remains low (< 0.5 wt.%), indicating preferential Br uptake. (b) Na-jarosite contains negligible halogens, with Br < 0.1 wt.% and Cl near zero. These results highlight strong A-site control, with Br and Cl incorporation suppressed in Na-jarosite. Error bars are smaller than symbols.

into jarosite were evaluated using partition values, defined as the ratio of halogen concentrations in the solid phase (wt.%) to those in the final solutions. Partition values ≥ 1 indicate preferential incorporation into jarosite, whereas values < 1 reflect retention in the aqueous phase.

At 25 °C under Fe^{2+} oxidation, K-jarosite exhibited strong Br^- incorporation, with partition values of 3.9–5.9 in Br-only systems and 4.5–20.1 in Br-Cl systems, while Cl^- values remained < 0.2 , indicating negligible uptake. In contrast, Na-jarosite incorporated much less Br^- (partition values 0.2–0.5) and effectively excluded Cl^- (partition values ~ 0) (Table 1). These results demonstrate that Br^- is far more compatible with jarosite than Cl^- , and that K-jarosite accommodates Br^- much more readily than its Na counterpart.

At 140 °C under Fe^{3+} forced hydrolysis, halogen partitioning was substantially reduced. For K-jarosite, Br partition values ranged from 0.4 to 0.8 across the tested concentration range, while Cl values remained < 0.1 (Table 2). This indicates that even at elevated temperatures and in halogen-rich solutions, Br was only moderately incorporated and Cl largely excluded. In contrast, Na-jarosite synthesized at 140 °C incorporated negligible halogens, with Br partition values consistently < 0.2 and Cl values essentially zero (Table 2). These results confirm the poor structural compatibility of Na-jarosite with halogens under both low- and high-temperature conditions.

Collectively, the partitioning behavior highlights fundamental crystallochemical controls: (1) Br^- has a much higher affinity for jarosite structures than Cl^- ; (2) K-jarosite incorporates Br^- far more efficiently than Na-jarosite; and (3) halogen incorporation decreases at higher synthesis temperatures, likely due to competition with OH^- or kinetic limitations on substitution.

3.3 Morphological and structural characterization of halogen-bearing jarosite

3.3.1 SEM observations

SEM imaging reveals distinct morphologies of jarosite synthesized under different conditions (Fig. 3). At 25 °C, K-jarosite shows a strong dependence on halogen content. The halogen-free sample (K-blank-25C) forms well-faceted euhedral crystals with rhombohedral or bipyramidal habits (Fig. 3(a)). In contrast, halogen-bearing samples develop more irregular and aggregated morphologies: the Br-only sample (K-Br-04) forms compact, partially dissolved aggregates (Fig. 3(b)); the Cl-only sample (K-Cl-04) yields small, irregular grains (Fig. 3(c)); and the Br-Cl mixed sample (K-Br,Cl-05) produces polycrystalline clusters of coarse and fine particles with surface dissolution features (Fig. 3(d)), suggesting halogen-induced growth inhibition or corrosion. In contrast, Na-jarosite retains relatively well-developed single crystals even in halogen-bearing

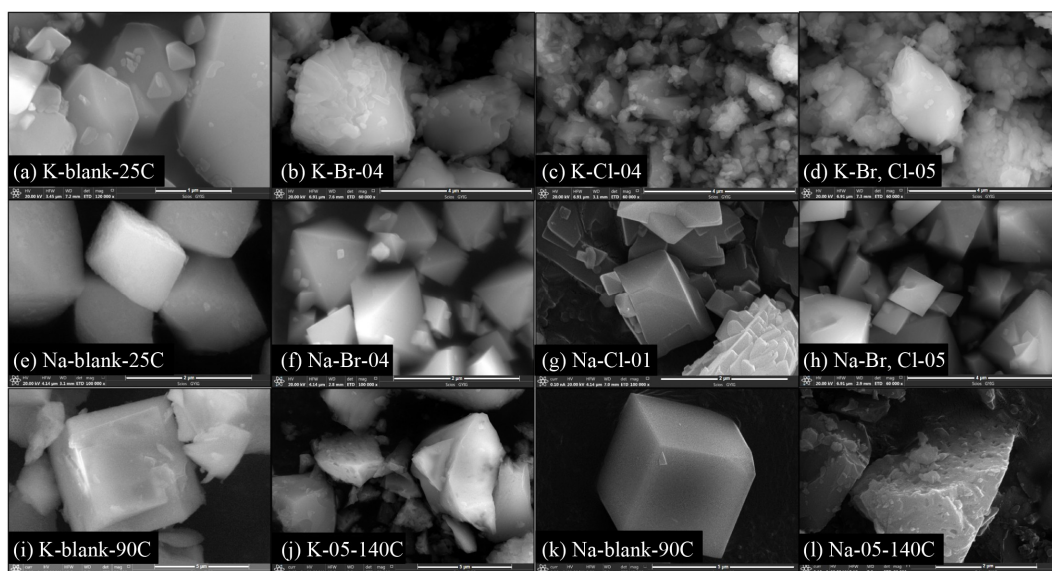


Fig. 3 Representative SEM images of jarosite synthesized at 25 °C (Fe^{2+} oxidation) and under hydrothermal conditions (Fe^{3+} hydrolysis). For each halogen-bearing group, the sample with the highest halogen content is shown. (a–d) K-jarosite at 25 °C; (a) blank yields euhedral crystals; (b) Br-only shows compact aggregates with partial dissolution; (c) Cl^- only forms smaller, irregular grains; (d) Br-Cl mixed displays polycrystalline aggregates with surface dissolution. (e–h) Na-jarosite at 25 °C; (e) blank produces well-defined rhombohedra; (f) Br-only shows sharp euhedral crystals; (g) Cl-only shows lamellar growth with clean surfaces; (h) Br-Cl mixed forms densely packed crystals. (i–l) Hydrothermal jarosite; (i) K-blank shows larger but slightly corroded crystals; (j) K-Br-Cl mixed forms rough aggregates with pitting; (k) Na-blank yields smooth rhombohedra; (l) Na-Br-Cl mixed produces poorly crystalline aggregates. Overall, halogen type, A-site cation, and synthesis temperature control morphology, with high Br and higher temperatures favoring irregular and aggregated textures.

systems. The blank (Na-blank-25C) forms large euhedral rhombohedra (Fig. 3(e)); both the Br-only (Na-Br-04) and Br-Cl mixed (Na-Br,Cl-05) samples preserve sharp, smooth crystal faces (Figs. 3(f), 3(h)); and the Cl-only sample (Na-Cl-01) develops flat lamellar surfaces, reflecting layered growth (Fig. 3(g)).

These features suggest that Na-jarosite is less sensitive to halogen-induced morphological disruptions than K-jarosite. One possible reason is that, compared to K-jarosite, Na-jarosite incorporates substantially lower halogen contents despite comparable halogen concentrations in solution, which may reflect both intrinsic structural constraints of the Na-jarosite lattice and the influence of higher Fe and sulfate concentrations in the initial solutions used for the Na-jarosite experiments.

Under hydrothermal conditions (90 or 140 °C), halogen-free jarosite forms well-developed euhedral crystals with relatively high crystallinity, whereas Br-Cl mixed systems yield products with diminished crystallinity, irregular morphologies, poorly developed faces, and enhanced aggregation or surface corrosion. For example, halogen-free K-jarosite at 90 °C (K-blank-90C) produces relatively large crystals with minor corrosion (Fig. 3(i)), while the Br-Cl-bearing sample at 140°C (K-05-140C) forms rough polycrystalline aggregates with surface pitting (Fig. 3(j)). Similarly, halogen-free Na-jarosite at 90°C (Na-blank-90C) develops well-defined rhombohedral crystals with smooth faces (Fig. 3(k)), whereas the Br-Cl-bearing sample at 140 °C (Na-05-140C) produces poorly crystalline aggregates lacking distinct habits (Fig. 3(l)).

Across both low-temperature and hydrothermal regimes, halogen-free jarosite typically exhibits well-defined crystal habits and high crystallinity. By contrast, high halogen concentrations in solution, particularly where substantial halogen incorporation occurs (as in K-jarosite), induce pronounced morphological changes, including aggregation, irregular crystal shapes, and surface dissolution. These patterns underscore the combined influence of synthesis pathway, halogen concentration, and A-site cation identity on jarosite crystal growth.

3.3.2 XRD patterns and Rietveld analysis of halogen-bearing jarosite

Figure 4 shows XRD patterns of selected K-jarosite synthesized at 25 °C and under hydrothermal conditions, illustrating the effects of halogen incorporation on primary diffraction peaks. At 25 °C, both Br-only and Br-Cl mixed samples display systematic peak shifts toward higher 2θ angles with increasing Br content, reflecting progressive lattice contraction. These shifts are most pronounced in low-temperature samples with higher Br incorporation. Under hydrothermal conditions (140 °C),

Br uptake was lower and the corresponding peak shifts were subtle but still detectable in the Br-Cl series.

Figure 5 presents the corresponding XRD patterns for Na-jarosite. At 25 °C, peak shifts to higher 2θ angles were also observed with increasing Br content, though the effect was weaker than in K-jarosite, consistent with the much lower Br incorporation. Under hydrothermal conditions, Na-jarosite peak positions remained essentially unchanged across the Br-Cl series, reflecting its limited halogen uptake. Overall, the XRD data show that Br incorporation induces lattice contraction, with K-jarosite being far more susceptible to halogen-related structural perturbations than Na-jarosite.

Consistently, Rietveld refinement of XRD data revealed systematic variations in jarosite unit cell parameters with increasing Br incorporation (Table 3). For K-jarosite at 25 °C, both Br-only and Br-Cl series showed a clear decrease in unit cell volume and c -axis length with rising Br content. The cell volume decreased from 796.12 Å³ in halogen-free jarosite to 790.49 Å³ in Br-only jarosite (11.24 wt.% Br) and 789.54 Å³ in Br-Cl jarosite (7.66 wt.% Br). The a parameter contracted slightly (from 7.3113 to 7.3007 Å), while the c parameter decreased more markedly (from 17.1973 to 17.1047 Å), indicating progressive lattice contraction. Under hydrothermal conditions, K-jarosite showed only minor and less systematic changes as Br contents varied from 0.08 to 2.94 wt.%, with cell volumes of 795.72 to 794.68 Å³ and c -axis values remaining near 17.20 Å, consistent with lower Br uptake and more stable crystallization.

For Na-jarosite, Br incorporation was much lower (typically < 1 wt.%). At 25 °C, samples showed only slight decreases in unit cell volume and lattice parameters with increasing Br. For instance, in the Br-only group, the cell volume decreased from 774.70 Å³ (blank) to 773.72 Å³ (0.79 wt.% Br), with the a parameter fluctuating slightly (~7.326-7.329 Å) and the c parameter increasing marginally (from 16.6176 to 16.6352 Å). Similar minor changes were observed in Br-Cl mixed Na-jarosite. In contrast, hydrothermal Na-jarosite exhibited no systematic variation, as Br contents were below detection limits in most cases. Unit cell volumes spanned from 769.51 to 774.63 Å³ without correlation to Br content, reflecting minimal structural response under these conditions.

Overall, these results indicate that Br incorporation into jarosite leads to subtle but consistent lattice contraction, particularly in K-jarosite synthesized at 25 °C, while Na-jarosite shows only minor structural changes due to its limited halogen uptake. These crystallographic trends are consistent with the observed XRD peak shifts.

3.3.3 Raman spectroscopic features

Raman spectra of representative K- and Na-jarosite

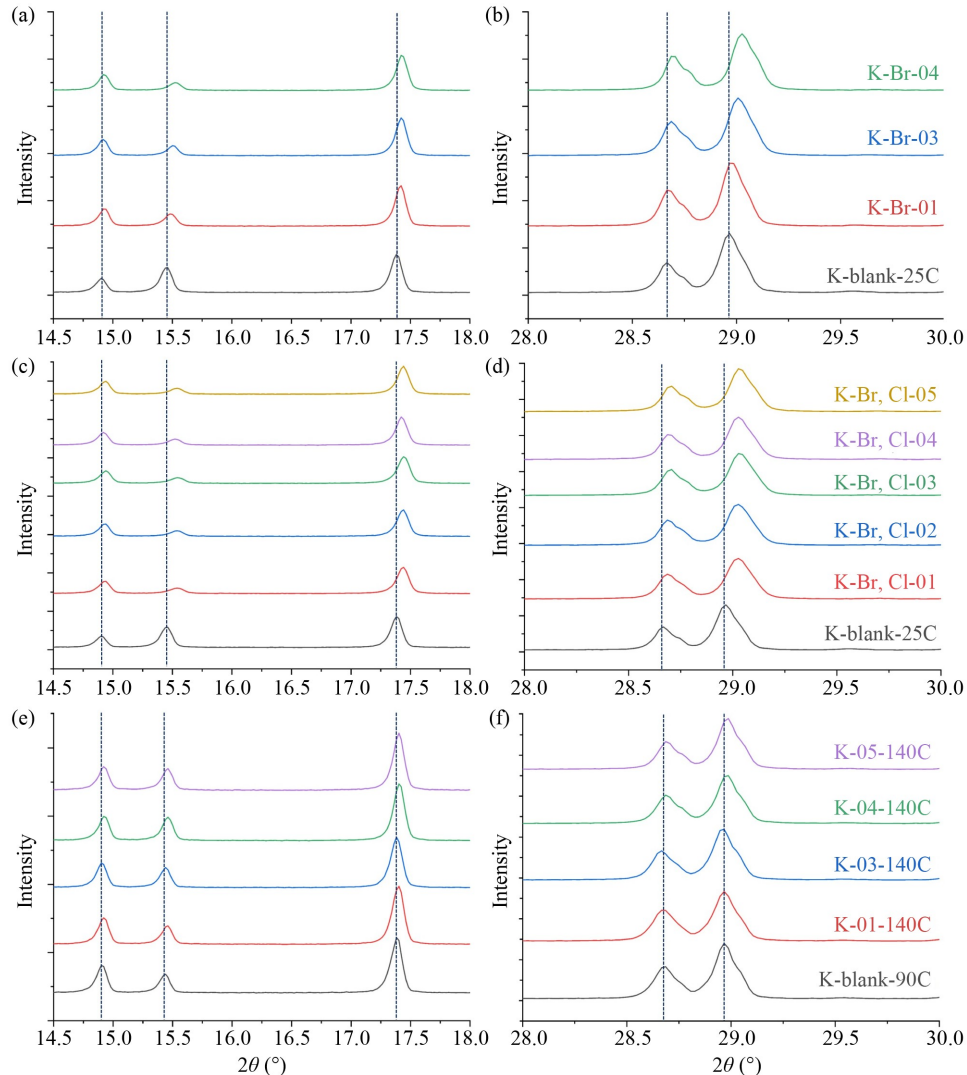


Fig. 4 XRD patterns of K-jarosite synthesized at 25 °C (a–d) and hydrothermally at 140 °C (e–f). Stacked profiles are ordered by increasing Br content. (a, b) Br-only; (c, d) Br-Cl mixed (25 °C); (e, f) Br-Cl mixed (140 °C). With higher halogen incorporation, major peaks (14.5°–18° and 28°–30° 2θ) systematically shift to higher angles, indicating unit-cell contraction due to Br substitution. The effect is most pronounced in low-temperature samples, consistent with their higher halogen uptake.

samples synthesized at 25 and 140 °C are shown in Figs. 6 and 7. The spectra are divided into three regions for analysis: 100–700 cm^{-1} (lattice modes), 950–1250 cm^{-1} (SO_4^{2-} vibrations), and 3300–3500 cm^{-1} (O–H stretching).

In the 100–700 cm^{-1} region, all samples, regardless of halogen content or synthesis condition, exhibited well-defined vibrational bands attributed to Fe–O bending and M–O–S (M = Fe, K or Na) lattice vibrations. Band positions and intensities remained consistent across halogen-free and halogen-bearing specimens.

In the 950–1250 cm^{-1} region, sharp peaks near 1010–1020 cm^{-1} correspond to the symmetric stretching (ν_1) vibrations of SO_4^{2-} , characteristic of well-crystallized jarosite. These peaks showed negligible shifts or broadening with increasing halogen content.

The most notable differences were found in the O–H

stretching region (3300–3500 cm^{-1}). Halogen-free samples displayed a prominent peak centered near 3375 cm^{-1} . In halogen-bearing samples, particularly those with higher Br^- or Cl^- contents, the peak intensity in this region decreased markedly, accompanied by broadening and, in some cases, lower signal-to-noise ratios. These changes were more pronounced in K-jarosite than in Na-jarosite, consistent with their differing halogen incorporation levels. No new peaks were observed in any region, and the spectra of hydrothermally synthesized samples followed similar trends, though signals in the OH region were generally weaker in Na-jarosite due to low halogen incorporation.

These results indicate that Br^- and Cl^- incorporation does not disrupt the jarosite lattice framework or sulfate coordination. Instead, the most significant spectral changes occur in the O–H stretching region, where

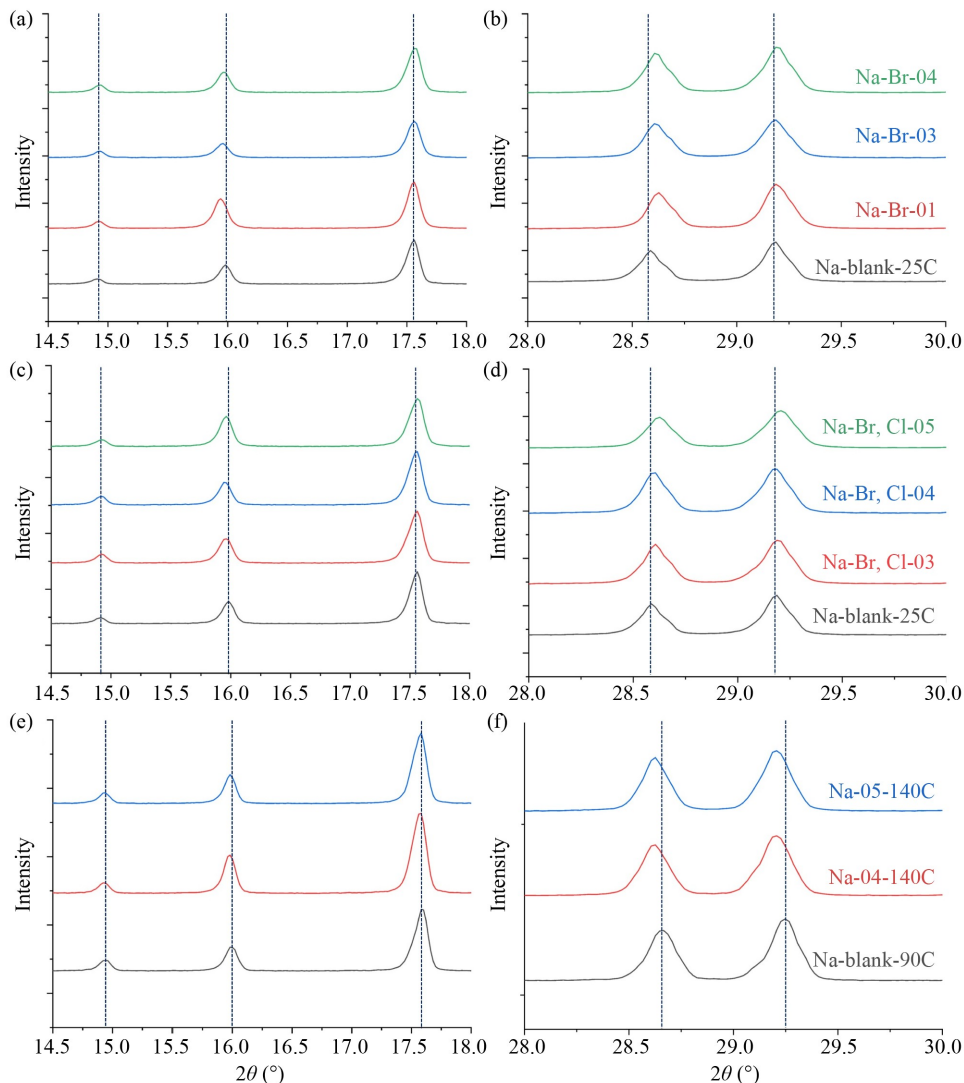


Fig. 5 XRD patterns of Na-jarosite synthesized at 25 °C (a–d) and hydrothermally at 140 °C (e–f). Profiles are ordered by increasing Br content, though overall halogen incorporation is lower than in K-jarosite. (a, b) Br-only; (c, d) Br-Cl mixed (25 °C); (e, f) Br-Cl mixed (140 °C). At 25 °C, diffraction peaks (14.5°–18° and 28°–30° 2θ) shift slightly to higher angles with Br addition, suggesting minor unit-cell contraction. Under hydrothermal conditions, shifts are minimal, reflecting much lower halogen uptake.

Table 3 Rietveld refinement results of K- and Na-jarosite samples with different Br contents

Samples	Br contents (wt.%)	Cell volume (\AA^3)	Crystal density (g/cm^3)	Lattice parameters a (\AA)	Lattice parameters c (\AA)	Rp	Rwp	Rexp	GOF
K-blank-25C	–	796.12(5)	3.1337(2)	7.3113(2)	17.1973(5)	4.51	6.26	2.98	2.10
K-Br-01	5.34	794.31(3)	3.14084(13)	7.30711(13)	17.1779(3)	4.79	6.54	2.99	2.19
K-Br-03	8.04	792.83(5)	3.1467(2)	7.3069(2)	17.1468(5)	4.38	6.06	3.00	2.02
K-Br-04	11.24	790.49(4)	3.15602(18)	7.30328(18)	17.1132(5)	4.49	6.16	3.01	2.05
K-blank-25C	–	796.12(5)	3.1337(2)	7.3113(2)	17.1973(5)	4.51	6.26	2.98	2.10
K-Br,Cl-01	1.06	790.72(9)	3.1551(4)	7.3050(4)	17.1100(9)	4.57	6.37	3.04	2.09
K-Br,Cl-02	1.80	790.87(8)	3.1545(3)	7.3059(3)	17.1092(8)	4.50	6.29	3.07	2.05
K-Br,Cl-03	3.27	790.98(7)	3.1541(3)	7.3055(3)	17.1132(7)	4.68	6.49	3.03	2.14
K-Br,Cl-04	5.68	790.12(5)	3.1575(2)	7.3028(2)	17.1073(5)	4.69	6.4	3.04	2.11
K-Br,Cl-05	7.66	789.54(5)	3.1598(2)	7.3007(2)	17.1047(5)	4.55	6.26	3.02	2.07
K-blank-90C	–	794.91(3)	3.13850(11)	7.30355(12)	17.2075(3)	4.81	6.76	3.09	2.19
K-01-140C	0.08*	795.44(3)	3.13640(12)	7.30609(12)	17.2070(3)	4.41	6.08	3.07	1.98
K-03-140C	0.41	795.04(3)	3.13796(11)	7.30562(11)	17.2007(3)	4.10	5.62	3.08	1.82

(continued)

Samples	Br contents (wt.%)	Cell volume (Å ³)	Crystal density (g/cm ³)	Lattice parameters <i>a</i> (Å)	Lattice parameters <i>c</i> (Å)	Rp	Rwp	Rexp	GOF
K-04-140C	1.09	795.72(3)	3.13527(11)	7.30700(11)	17.2089(3)	4.54	6.12	3.06	2.00
K-05-140C	2.94	794.68(3)	3.13938(10)	7.30368(10)	17.2020(3)	4.22	5.58	3.04	1.83
Na-blank-25C	–	774.70(8)	3.1168(3)	7.3370(3)	16.6176(7)	4.46	6.05	2.89	2.09
Na-Br-01	0.14*	773.71(12)	3.1207(5)	7.3245(5)	16.6531(11)	4.51	6.34	2.86	2.22
Na-Br-03	0.53	774.72(6)	3.1167(3)	7.3292(3)	16.6534(6)	4.09	5.41	2.85	1.90
Na-Br-04	0.79	773.72(5)	3.1207(2)	7.3285(2)	16.6352(5)	4.39	6.03	2.87	2.10
Na-blank-25C	–	774.70(8)	3.1168(3)	7.3370(3)	16.6176(7)	4.46	6.05	2.89	2.09
Na-Br,Cl-03	0.07*	772.93(6)	3.1239(2)	7.3263(2)	16.6282(6)	4.44	6.09	2.87	2.12
Na-Br,Cl-04	0.21*	773.11(5)	3.1232(2)	7.3269(2)	16.6294(5)	4.40	6.03	2.86	2.10
Na-Br,Cl-05	0.43	773.01(7)	3.1236(3)	7.3256(3)	16.6332(7)	4.62	6.40	2.87	2.23
Na-blank-90C	–	769.51(6)	3.1378(2)	7.3167(2)	16.5982(6)	4.76	6.56	3.00	2.19
Na-04-140C	0.03*	772.57(11)	3.1253(4)	7.3261(5)	16.6211(10)	4.59	6.31	2.94	2.15
Na-05-140C	0.08*	774.63(10)	3.1171(4)	7.3326(4)	16.6359(10)	4.20	5.73	2.96	1.94

Notes: Values marked with an asterisk indicate measurements below the detection limits (0.35 wt% for Br by the XRF). However, these values are included in the table due to their good linear correlation with the initial solution concentrations. Rp = R-pattern, Rwp = weighted-pattern, Rexp = R-expected, GOF = Goodness of fit = Rwp/Rexp.

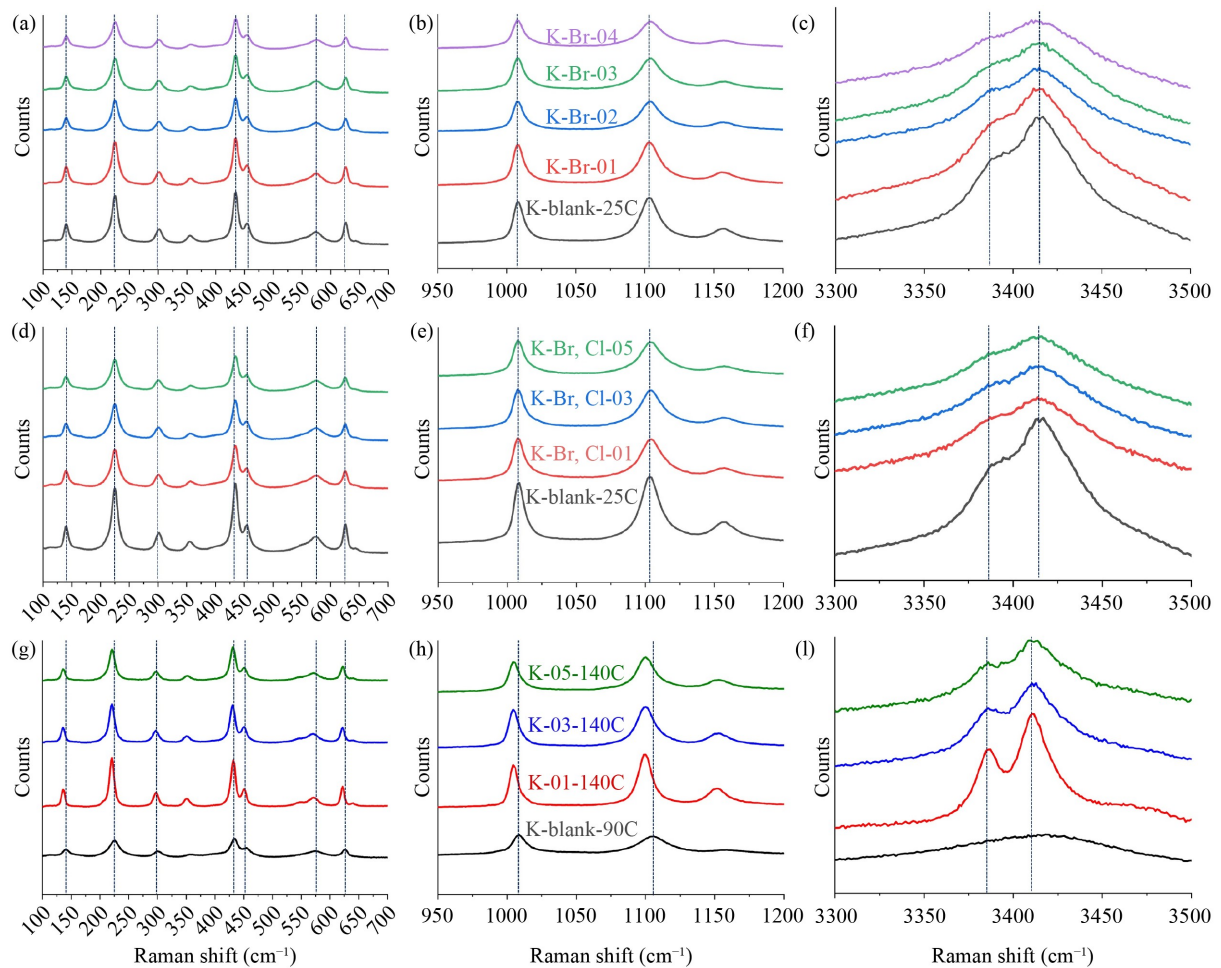


Fig. 6 Raman spectra of K-jarosite synthesized at 25 and 140 °C, showing responses to halogen incorporation. (a–c) Br-only (25 °C); (d–f) Br-Cl mixed (25 °C); (g–i) Br-Cl mixed (140 °C). Panels (a, d, g): 100–700 cm⁻¹ (lattice vibrations); (b, e, h): 950–1250 cm⁻¹ (SO₄²⁻ symmetric stretch); (c, f, i): 3300–3500 cm⁻¹ (O–H stretch). Spectra are stacked by increasing halogen content (bottom = blank). Lattice and sulfate bands show minimal changes, whereas the O–H region broadens and weakens, indicating OH⁻ substitution by halogens.

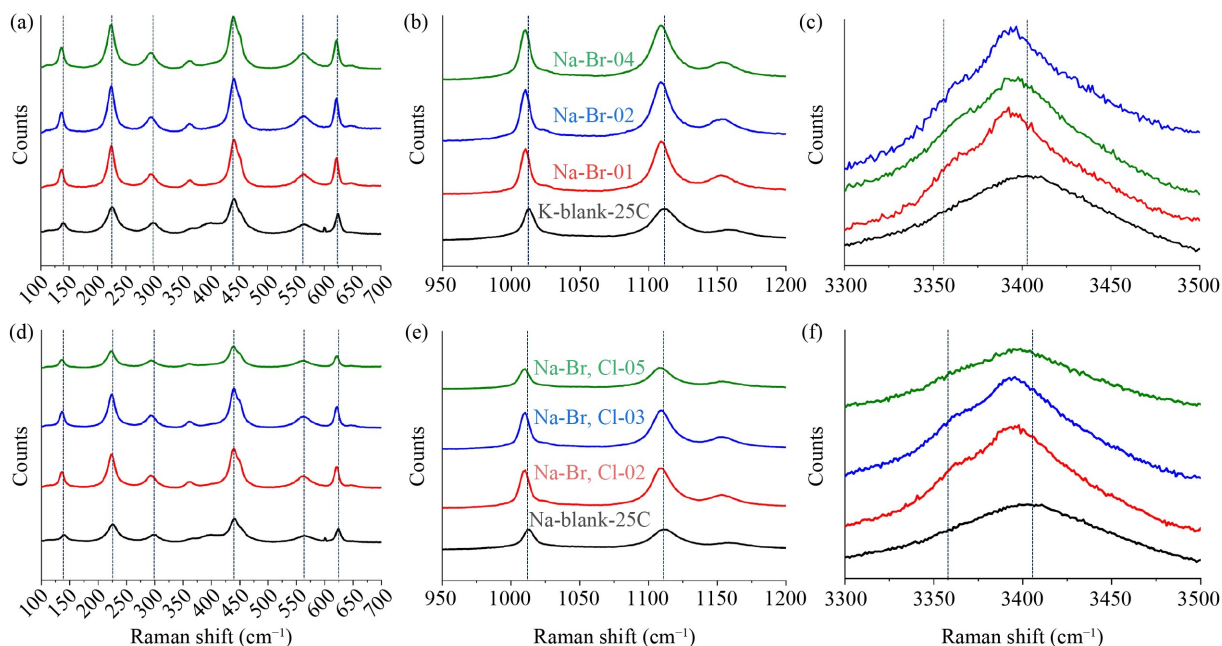


Fig. 7 Raman spectra of Na-jarosite synthesized at 25 °C, showing spectral responses to halogen incorporation. (a–c) Br-only samples; (d–f) Br-Cl mixed samples. Hydrothermal samples are excluded due to negligible halogen content. (a, d): 100–700 cm^{-1} (lattice vibrations, Fe–O bending, M–O–S framework). (b, e): 950–1200 cm^{-1} (SO_4^{2-} ν_1 symmetric stretching). (c, f): 3300–3500 cm^{-1} (O–H stretching). Spectra are stacked from bottom to top with increasing halogen content, the bottom being halogen-free. Lattice and sulfate bands show little variation, indicating Br[−]/Cl[−] do not alter the framework or SO_4^{2-} environment. In contrast, the O–H band near 3375 cm^{-1} decreases with higher halogen levels, suggesting substitution at OH[−] sites under low-temperature conditions.

systematic peak attenuation and broadening with increasing halogen content suggest substitution of OH[−] groups by Br[−] and Cl[−].

4 Discussion

4.1 Synthetic temperature and alkali cation effects on halogen incorporation

Our findings demonstrate that halogen incorporation in jarosite is strongly dependent on both the A-site cation type and synthesis temperature. K⁺ promotes a more robust jarosite framework and enables substantial Br[−] incorporation, especially under low-temperature conditions. This capacity is not simply a result of improved crystallinity; rather, it reflects the more accommodating structure of K-jarosite, likely stemming from greater A-site stability and a higher tolerance for lattice defects.

In contrast, Na-jarosite consistently shows limited halogen uptake, even at high Br[−] concentrations in solution. This intrinsic limitation persists across synthesis temperatures and likely reflects less favorable environments for OH[−] substitution, perhaps due to stronger hydrogen bonding networks or lower structural flexibility around the A-site. Importantly, this occurs

despite Na-jarosite exhibiting good crystallinity in both XRD and Raman analyses, indicating that halogen exclusion is not a crystallographic artifact but arises from structural or energetic constraints.

Temperature also exerts a strong influence. At low temperature, K-jarosite incorporates more Br[−], likely facilitated by slower crystal growth kinetics and enhanced defect trapping. Under hydrothermal conditions, increased structural ordering reduces halogen uptake, suggesting that rapid, ordered growth suppresses anion substitution. Overall, these findings underscore that both alkali cation identity and crystallization regime are key factors controlling halogen incorporation pathways in jarosite.

4.2 Substitution sites of bromide and chloride in jarosite and structural changes

Compositional, crystallographic, and spectroscopic evidence collectively indicate that halogen incorporation in jarosite, particularly in K-jarosite, occurs primarily through substitution at hydroxyl (OH[−]) sites. In contrast, Na-jarosite retains nearly complete OH₆ coordination and incorporates only trace halogens even under high halogen availability. This contrast highlights the greater structural flexibility and anion substitution capacity of K-jarosite, likely reflecting more stable A-site configurations and enhanced defect accommodation.

XRD results further support OH⁻ substitution. With increasing halogen content, the primary diffraction peaks of K-jarosite systematically shift toward higher 2θ angles, indicating unit-cell contraction, especially along the *c*-axis. Rietveld refinement confirms a consistent decrease in the *c* parameter, consistent with substitution at the apical OH⁻ sites of FeO₆ octahedra. Although Br⁻ and Cl⁻ are larger than OH⁻, their incorporation likely disrupts local hydrogen bonding, leading to subtle structural compaction.

Raman spectroscopy provides additional confirmation. The characteristic OH-stretching band near 3375 cm⁻¹ becomes progressively weakened and broadened with increasing Br⁻ or Cl⁻ in K-jarosite, without generating new vibrational modes. These changes are absent in halogen-free controls and only weakly developed in Na-jarosite, indicating that halogen substitution perturbs hydrogen bonding without introducing new structural units.

Taken together, these results demonstrate that Br⁻ and Cl⁻ incorporation in jarosite occurs dominantly via OH⁻ substitution, a process strongly favored in the structurally permissive K-jarosite system, particularly under low-temperature conditions.

4.3 Enrichment of Br⁻ in low-temperature jarosite and double salt systems

Building on earlier studies (Chang and Zhao, 2018; Zhao et al., 2014), this work provides direct experimental confirmation that Br⁻ can be incorporated into jarosite, particularly in low-temperature K-jarosite. Previous investigations based on in situ observations and laboratory experiments had suggested this possibility, but quantitative constraints were limited.

Here we present the first systematic experimental evidence that Br⁻ can be strongly enriched in K-jarosite precipitated at 25 °C, with solid-liquid partition values (C_{s-Br}/C_{aq-Br}) reaching up to 18.12. This degree of enrichment departs from the commonly assumed conservative behavior of halogens in dilute systems and points to a selective uptake mechanism, most likely through OH⁻ substitution facilitated by slow crystallization kinetics and enhanced structural flexibility of the K-jarosite framework.

Interestingly, similar Br enrichment has been reported in the double salt kainite (KMg(SO₄)Cl·3H₂O), which forms during evaporation of marine bitterns (Siemann and Schramm, 2002). At low initial Br concentrations, kainite preferentially incorporates Br⁻, removing over 25% of Br from the residual brine (Siemann and Schramm, 2002). This effect diminishes at higher Br levels, suggesting that Br uptake is governed by kinetic trapping and crystallization conditions rather than equilibrium partitioning. Although kainite is rare on Earth, spectral analyses of surface materials at Gusev

Crater indicate its possible occurrence on Mars (Rice et al., 2010), raising the prospect that Br-rich double salts may form under cold, saline Martian conditions.

The enrichment of Br⁻ in both K-jarosite and kainite appears to be driven by distinct but complementary mechanisms. In K-jarosite, Br⁻ substitutes directly for OH⁻ in the crystal lattice, as shown in this study. In kainite, Br⁻ incorporation likely occurs through coprecipitation with KBr or MgBr₂·6H₂O, or possibly via substitution at Cl⁻ sites, reflecting a less structurally constrained mode of uptake. Together, these findings suggest that certain low-temperature K-bearing sulfate and double-salt systems may serve as effective geochemical sinks for Br⁻ in Martian evaporitic environments. Such mineral hosts could generate localized Br enrichment (Zhao et al., 2014) and contribute to halogen cycling on the Martian surface through brine-salt interactions.

5 Implications for Mars

5.1 Distribution and formation conditions of jarosite on Mars and Earth

Natural jarosite occurrence on both Earth and Mars provide critical context for interpreting the experimental results of this study. On Mars, jarosite has been definitively detected at two major landing sites: Meridiani Planum and Gale Crater. At Meridiani Planum, Opportunity rover data revealed abundant jarosite associated with the sulfate-rich Burns Formation (Morris et al., 2006; Rieder et al., 2004). Spectral and chemical analyses indicate that the jarosite is primarily Na-dominant (i.e., Na⁺ > K⁺ > H₃O⁺), with little to no coprecipitated goethite, and is interpreted to have formed under low-temperature, oxidizing, and chemically evolved brine conditions. This is particularly notable given our experimental observation that phase-pure Na-jarosite is difficult to synthesize at low temperature and requires elevated Fe and sulfate concentrations. The natural formation of Na-jarosite without goethite implies a unique aqueous environment capable of sustaining high Fe³⁺ and SO₄²⁻ activity in solution without an apparent K source, otherwise K-jarosite would be preferentially precipitated.

In contrast, jarosite detected by the Curiosity rover in the lower Murray Formation of Gale Crater appears to be K-dominant (Martin et al., 2017). Based on the K-Ar dating results, the jarosite in the Mojave 2 mudstone is interpreted to have formed from post-depositional diagenetic fluids during the Amazonian period, rather than from primary sulfate precipitation in Gale Lake (Martin et al., 2017). This aligns well with our experimental results showing that K-jarosite forms more

readily and consistently under both low- and high-temperature conditions. The greater thermodynamic stability and crystallization kinetics of K-jarosite, as well as its enhanced ability to incorporate halogens, suggest that the fluid conditions in Gale Crater may have differed substantially from those in Meridiani Planum.

Thermodynamic data further support the preferential formation of K-jarosite. Among jarosite endmembers, $\text{KFe}_3(\text{SO}_4)_2(\text{OH})_6$ has the most negative standard Gibbs free energy of formation ($\Delta G^\circ_f = -3309.8$ kJ/mol) at 25 °C, compared with $\text{NaFe}_3(\text{SO}_4)_2(\text{OH})_6$ (-3256.7 kJ/mol) (Drouet and Navrotsky, 2003). This trend confirms that K-jarosite is the thermodynamically most stable phase, providing a strong energetic driving force for its preferential nucleation and crystallization over the Na analog under otherwise identical conditions.

This thermodynamic advantage is consistent with our experimental findings: K-jarosite readily forms phase-pure, well-crystallized solids with near-ideal Fe occupancy and high halogen uptake capacity, while Na-jarosite remains deficient in Fe and exhibits limited halogen incorporation despite similar crystallinity. The greater exergonicity of K-jarosite formation may not only promote structural development but also facilitate anion substitution (e.g., OH^- by Br^-), explaining the observed disparity in halogen behavior between the two systems.

On Earth, jarosite is typically found in modern acid-sulfate environments such as acid mine drainage and hydrothermal alteration zones. It is rarely preserved in ancient geological records, likely due to its metastability and susceptibility to transformation into more stable Fe oxides during diagenesis (Ren and Vasconcelos, 2020; Zuo et al., 2021). Interestingly, terrestrial jarosite samples generally exhibit minimal solid solution behavior, most crystallize as near-endmember compositions (Desborough et al., 2010). K is the dominant A-site cation in most natural samples, reflecting the higher thermodynamic favorability of K-jarosite over Na-jarosite. Several factors likely contribute to the lack of solid solution, including the presence of solvus in both supergene and hydrothermal systems, post-depositional recrystallization, hydrothermal overprinting, or limited coexisting A-site cation diversity during formation. Diagenesis may also selectively alter Na-rich jarosite, replacing them with secondary phases or transforming them into K-rich forms, further suppressing solid-solution development in natural settings. In addition, terrestrial hydronium-bearing jarosite likely is unstable over geologic timescales (Desborough et al., 2010).

These comparisons highlight how Martian jarosite compositions and distributions, particularly the presence of Na-jarosite in Burns Formation, can potentially serve as indicators of highly acidic, high ionic strength, sulfate-rich brine conditions capable of stabilizing unusual mineral species. These findings underscore the diagnostic potential of jarosite composition for reconstructing paleo-

fluid chemistry and diagenetic pathways on Mars.

5.2 Halogen behavior in jarosite and implications for Mars-returned samples

Synthetic K-jarosite demonstrates superior structural integrity, more complete Fe- and A-site occupancy, and a greater capacity for halogen incorporation than Na-jarosite under both low- and high-temperature conditions. These structural differences provide a geochemical framework for interpreting natural jarosite formation and anticipating their halogen-bearing behavior in terrestrial and extraterrestrial settings, particularly on Mars.

Our experiments show pronounced Br^- enrichment in low-temperature K-jarosite, with solid-liquid partition values ($C_{s-\text{Br}}/C_{\text{aq}-\text{Br}}$) reaching 18.12. This behavior contrasts sharply with the widely held expectation that halogens, especially in dilute solutions, behave conservatively and remain predominantly in the aqueous phase. Instead, Br^- shows a strong preference for incorporation into jarosite solids, even at relatively low initial solution concentrations (e.g., 0.07 wt.% in this study). Such enrichment suggests that selective uptake is not controlled solely by equilibrium solubility but is strongly influenced by structural substitution pathways and crystallization kinetics.

Although jarosite is a sulfate rather than a double salt, this behavior parallels findings in synthetic kainite ($\text{KMg}(\text{SO}_4)\text{Cl}\cdot 3\text{H}_2\text{O}$), where Br^- also exhibited unexpected enrichment at low initial concentrations. In those experiments, kainite precipitating from evaporating Cl^-/Br^- solutions incorporated Br^- preferentially into its structure despite Br^- being a minor anion in solution (Siemann and Schramm, 2002). These results suggest that sulfate-bearing mineral systems with structural compatibility for large halide ions (e.g., jarosite, kainite) may act as selective Br sinks in low-temperature evaporitic environments.

The enrichment of Br^- in both systems likely reflects two complementary factors: 1) the availability of structurally flexible anion sites, particularly hydroxyl or coordinated water positions in jarosite, that can be substituted by halides, and 2) crystallization conditions (low temperature, high ionic strength) that promote defect formation or kinetic trapping of trace ions during rapid or incomplete mineral growth. In K-jarosite, Br^- appears to partially substitute for OH^- , as evidenced by Raman broadening in the OH-stretch region and consistent XRD lattice contraction. In kainite, Br^- is more likely accommodated through Cl^- substitution or hydration shells associated with Mg^{2+} , reflecting the structural tolerance of the double-salt framework.

These findings collectively suggest that low-temperature precipitation of K- and SO_4^{2-} -bearing minerals, whether jarosite or hydrated double salts, can serve as an efficient geochemical sink for Br^- on

planetary surfaces. Such a mechanism may help explain the Br variations observed in Martian surface materials (e.g., Rieder et al., 2004), where evaporation-driven assemblages formed under cold, chemically complex aqueous conditions. This also raises the possibility that Br-bearing jarosite or Br-rich double salts constitute important near-surface halogen reservoirs on Mars, with implications for reconstructing its fluid history and geochemical cycles.

These insights are particularly significant for future Mars-returned sample analysis. If jarosite is recovered in returned materials, it could serve not only as a geochronometer through K-Ar dating to constrain the timing of fluid activity, but also as a proxy for paleo-fluid chemistry and environmental conditions. Specifically, 1) halogen contents, especially Br^- , may reflect early diagenetic fluid compositions; 2) variations in lattice parameters, particularly *c*-axis contraction, can quantify halogen substitution; and 3) crystallinity and Fe occupancy provide constraints on formation temperature and the distinction between primary versus alteration products. Our results thus highlight the importance of sulfates (e.g., jarosite) and double salts (e.g., kainite) in future Mars-returned sample investigations, as they record not only the physicochemical properties of aqueous environments but also the pathways of halogen incorporation and cycling in early Martian brine systems.

6 Conclusions

Jarosite-group sulfates are common in acidic, sulfate-rich environments on both Earth and Mars, yet their role in halogen cycling remains poorly understood. In this study, we conducted a series of low- and high-temperature synthesis experiments to systematically investigate the partitioning behavior, structural incorporation, and crystallographic effects of Br^- and Cl^- in K- and Na-jarosite. Chemical, spectroscopic, and crystallographic analyses were used to quantify halogen uptake and identify the dominant substitution mechanisms.

1) Br^- is preferentially incorporated into K-jarosite, particularly at low temperatures. Jarosite synthesized at 25 °C via Fe^{2+} oxidation incorporates significant Br^- , with partition ratios ($C_{\text{s-Br}}/C_{\text{aq-Br}}$) exceeding 18, while Cl^- remains largely excluded. In contrast, Na-jarosite exhibits minimal halogen uptake under all tested conditions.

2) Halogen substitution occurs primarily at structural OH^- sites. Raman spectroscopy, XRD lattice shifts, and chemical analyses collectively indicate that Br^- and Cl^- substitute for hydroxyl groups in jarosite, resulting in contraction of the unit cell, most prominently in low-temperature K-jarosite.

3) Halogen incorporation is strongly modulated by alkali cation and synthesis temperature. K^+ -bearing jarosite accommodates more halogen than its Na analog.

Low-temperature conditions may promote Br^- uptake via defect trapping and slower crystallization kinetics, whereas hydrothermal synthesis enhances crystallinity but reduces halogen incorporation.

4) Br^- enrichment in K-jarosite mirrors that observed in evaporitic double salts (e.g., kainite), identifying it as a key Br^- sink. This behavior suggests that Br-bearing jarosite on Mars may record cold, acidic, and chemically evolved brine environments.

These findings underscore the dual role of jarosite as both a paleoenvironmental archive and an active participant in halogen cycling on early Mars. Variations in its crystallinity, lattice parameters, and halogen content may offer critical constraints for reconstructing ancient fluid conditions in future Mars sample return missions.

Acknowledgments

We gratefully acknowledge Bing Mo and Rui Li for their assistance with SEM analysis. Special thanks to Wei Du for her support with XRD analysis, which was essential for interpreting the crystallographic behavior of halogen-bearing jarosite. We also thank Wen Liang for his valuable insights into the interpretation of structural data and their relevance to anion substitution mechanisms. Changqing Liu and Zongcheng Ling are sincerely appreciated for their helpful discussions throughout the course of this study. This work was supported by the National Natural Science Foundation of China (Grant Nos. 41673072 and 42441803). We thank Fengke Cao and Xiaowen Yu for their valuable comments and suggestions, which helped us to greatly improve this manuscript.

Declaration of competing interest

Authors declare that they have no competing interests.

Data and materials availability

All the data generated and analyzed during this study are included in the published article. The XRD and Raman source data are available at the Science Data Bank, <https://doi.org/10.57760/sciencedb.29468>.

References

- Basciano L C, Peterson R C (2008). Crystal chemistry of the natrojarosite-jarosite and natrojarosite-hydronium jarosite solid-solution series: A synthetic study with full Fe site occupancy. *Am Mineral*, 93(5–6): 853–862
- Belleau-Magnat G, Lemelin M, Cloutis E, L  veill   R (2025).

- Mineralogy, geochemistry and morphology of Arctic gossans on Axel Heiberg Island, NU, Canada: Spectroscopic investigation and implications for Mars. *Planet Space Sci*, 256: 106036
- Carson G L, McHenry L J, Hynek B M, Cameron B I, Glenister C T (2023). Mineralogy and bulk geochemistry of a fumarole at Hverir, Iceland: Analog for acid-sulfate leaching on Mars. *Am Mineral*, 108(3): 409–429
- Chang R, Zhao Y (2018). Partitioning behavior of Br and Cl during jarosite precipitation and its implications for sedimentary rock on Mars. *Kexue Tongbao*, 63(4): 461–470
- Desborough G A, Smith K S, Lowers H A, Swayze G A, Hammarstrom J M, Diehl S F, Leinz R W, Driscoll R L (2010). Mineralogical and chemical characteristics of some natural jarosites. *Geochim Cosmochim Acta*, 74(3): 1041–1056
- Driscoll R L, Leinz R W (2005). Methods for synthesis of some jarosites: U. S. Geological Survey Techniques and Methods, U. S. Geological Survey, Reston, Virginia.
- Drouet C, Navrotsky A (2003). Synthesis, characterization, and thermochemistry of K-Na-H₃O jarosites. *Geochim Cosmochim Acta*, 67(11): 2063–2076
- Farrand W H, Glotch T D, Rice J W Jr, Hurowitz J A, Swayze G A (2009). Discovery of jarosite within the Mawrth Vallis region of Mars: Implications for the geologic history of the region. *Icarus*, 204(2): 478–488
- Grasby S E, Percival J B, Bilot I, Ardakani O H, Smith I R, Galloway J, Bingué M, McLoughlin-Coleman T (2022). Extensive jarosite deposits formed through auto-combustion and weathering of pyritiferous mudstone, Smoking Hills (Ingniryuat), Northwest Territories, Canadian Arctic - A potential Mars analogue. *Chem Geol*, 587: 120634
- Hong H L, Liu C, Algeo T J, Rampe E B (2024). Jarosite formation in Permian-Triassic strata at Xiakou (South China): Implications for jarosite precipitation from HS upwelling on Mars. *Am Mineral*, 109(9): 1535–1544
- Klingelhöfer G, Morris R V, Bernhardt B, Schröder C, Rodionov D S, de Souza P A, Yen A, Gellert R, Evlanov E N, Zubkov B, Foh J, Bonnes U, Kankeleit E, Gütllich P, Ming D W, Renz F, Wdowiak T, Squyres S W, Arvidson R E (2004). Jarosite and hematite at Meridiani Planum from Opportunity's Mossbauer spectrometer. *Science*, 306(5702): 1740–1745
- Knight A L, Mitra K, Catalano J G (2024). Transformation of precursor iron(III) minerals in diagenetic fluids: potential origin of gray hematite at Vera Rubin Ridge. *J Geophys Res Planets*, 129(4): e2023JE007931
- Ling Z C, Cao F K, Ni Y H, Wu Z C, Zhang J, Li B (2016). Correlated analysis of chemical variations with spectroscopic features of the K-Na jarosite solid solutions relevant to Mars. *Icarus*, 271: 19–29
- Liu Y, Goudge T A, Catalano J G, Wang A (2018). Spectral and stratigraphic mapping of hydrated minerals associated with interior layered deposits near the southern wall of Melas Chasma, Mars. *Icarus*, 302: 62–79
- Madden M E E, Bodnar R J, Rimstidt J D (2004). Jarosite as an indicator of water-limited chemical weathering on Mars. *Nature*, 431(7010): 821–823
- Martin P E, Farley K A, Baker M B, Malespin C A, Schwenzer S P, Cohen B A, Mahaffy P R, McAdam A C, Ming D W, Vasconcelos P M, Navarro-González R (2017). A two-step k-ar experiment on Mars: dating the diagenetic formation of Jarosite from Amazonian groundwaters. *J Geophys Res Planets*, 122(12): 2803–2818
- Milliken R E, Swayze G A, Arvidson R E, Bishop J L, Clark R N, Ehlmann B L, Green R O, Grotzinger J P, Morris R V, Murchie S L, Mustard J F, Weitz C (2008). Opaline silica in young deposits on Mars. *Geology*, 36(11): 847–850
- Morris R V, Klingelhöfer G, Schröder C, Rodionov D S, Yen A, Ming D W, de Souza P A Jr, Wdowiak T, Fleischer I, Gellert R, Bernhardt B, Bonnes U, Cohen B A, Evlanov E N, Foh J, Gütllich P, Kankeleit E, McCoy T, Mittlefehldt D W, Renz F, Schmidt M E, Zubkov B, Squyres S W, Arvidson R E (2006). Mossbauer mineralogy of rock, soil, and dust at Meridiani Planum, Mars: Opportunity's journey across sulfate-rich outcrop, basaltic sand and dust, and hematite lag deposits. *J Geophys Res*, 111(E12): 2006JE00279
- Papike J J, Karner J M, Shearer C K (2006). Comparative planetary mineralogy: Implications of martian and terrestrial jarosite. A crystal chemical perspective. *Geochim Cosmochim Acta*, 70(5): 1309–1321
- Rampe E B, Ming D W, Blake D F, Bristow T F, Chipera S J, Grotzinger J P, Morris R V, Morrison S M, Vaniman D T, Yen A S, Achilles C N, Craig P I, Des Marais D J, Downs R T, Farmer J D, Fendrich K V, Gellert R, Hazen R M, Kah L C, Morookian J M, Peretyazhko T S, Sarrazin P, Treiman A H, Berger J A, Eigenbrode J, Fairén A G, Forni O, Gupta S, Hurowitz J A, Lanza N L, Schmidt M E, Siebach K, Sutter B, Thompson L M (2017). Mineralogy of an ancient lacustrine mudstone succession from the Murray formation, Gale crater, Mars. *Earth Planet Sci Lett*, 471: 172–185
- Rampe, E. B., Blake D F, Bristow T F, Ming D W, Vaniman D T, Morris R V, Achilles C N, Chipera S J, Morrison S M, Tu V M, Yen A S, Castle N, Downs G W, Downs R T, Grotzinger J P, Hazen R M, Treiman A H, Peretyazhko T S, Des Marais D J, Walroth R C, Craig P I, Crisp J A, Lafuente B, Morookian J M, Sarrazin P C, Thorpe M T, Bridges J C, Edgar L A, Fedo C M, Freissinet C, Gellert R, Mahaffy P R, Newsom H E, Johnson J R, Kah L C, Siebach K L, Schieber J, Sun V Z, Vasavada A R, Wellington D, Wiens R C (2020). Mineralogy of Vera Rubin Ridge From the Mars Science Laboratory CheMin Instrument, *J Geophys Res-Planet*, 125, e2019JE006306
- Ren Z, Vasconcelos P M (2020). Mechanisms and kinetics of argon diffusion in hypogene and supergene jarosites: Implications for geochronology and surficial geochemistry on Earth and Mars. *Geochim Cosmochim Acta*, 289: 207–224
- Rice M S, Bell J F III, Cloutis E A, Wang A, Ruff S W, Craig M A, Bailey D T, Johnson J R, de Souza P A Jr, Farrand W H (2010). Silica-rich deposits and hydrated minerals at Gusev Crater, Mars: Vis-NIR spectral characterization and regional mapping. *Icarus*, 205(2): 375–395
- Rieder R, Gellert R, Anderson R C, Brückner J, Clark B C, Dreibus G, Economou T, Klingelhöfer G, Lugmair G W, Ming D W, Squyres S W, d'Uston C, Wänke H, Yen A, Zipfel J (2004). Chemistry of rocks and soils at Meridiani Planum from the Alpha Particle X-ray

- spectrometer. *Science*, 306(5702): 1746–1749
- Siemann M G, Schramm M (2002). Henry's and non-Henry's law behavior of Br in simple marine systems. *Geochim Cosmochim Acta*, 66(8): 1387–1399
- Zhao Y Y S, McLennan S M, Schoonen M A A (2014). Behavior of bromide, chloride, and phosphate during low-temperature aqueous Fe(II) oxidation processes on Mars. *J Geophys Res Planets*, 119(5): 998–1012
- Zhou D S, Yu X W, Chang R, Zhao Y Y S, Li X Y, Liu J Z, Lin H L, Qi C (2022). Effects of formation pathways and bromide incorporation on Jarosite dissolution rates: implications for Mars. *J Geophys Res Planets*, 127(6): e2022JE007202
- Zuo P F, Sun J T, Liu X F, Hao J H, Zheng D S, Li Y (2021). Two types of jarosite in the early Cambrian sedimentary rocks: Insights for genesis and transformation of jarosite on Mars. *Icarus*, 369: 114651